Attahadi Medical Journal
2026;3(3):358-370
https://doi.org/10.69667/amj.26314

OPEN ACCESS

Original article

Enaminones as Versatile Building Blocks for Heterocyclic Synthesis: Novel Routes to 5-Nitrobenzofuran-Based Pyridine Analogues and Evaluation of Their Antimicrobial Activity, Molecular Docking

Hussniya AlDifar*, Basma Baaiu, Fakhri Elabbar

Department of Chemistry, Faculty of Science, Benghazi, University of Benghazi, P.O. Box 1308, Benghazi, Libya.
Corresponding Email. *Hussnya.difar@uob.edu.ly*

Keywords.
Enaminone, 5-nitrobenzofuran, Pyridine, Nicotinonitrile, Thioether, Antimicrobial Activity, Molecular Docking.

A B S T R A C T

A concise and efficient synthetic strategy was developed for the construction of a new family of 5-nitrobenzofuran-based pyridine, dihydropyridine, and pyridinyl thioether derivatives using a single enaminone intermediate as the central building block. The key enaminone, (E)-3-(dimethylamino)-1-(5-nitrobenzofuran-2-yl)prop-2-en-1-one (3), was prepared by condensation of 1-(5-nitrobenzofuran-2-yl)ethan-1-one (1) with N, N-dimethylformamide dimethyl acetal (DMF-DMA, 2) in dry xylene. Treatment of 3 with a range of active-methylene and 1,3-dicarbonyl reagents in the presence of ammonium acetate furnished the substituted pyridines 5–7, the 2-aminonicotinonitrile 9, the dihydropyridine carboxylate 10 and the 2-thioxopyridine-3-carbonitrile 11. The thione 11 was further S-functionalised with phenacyl bromide, chloroacetone and methyl iodide to deliver the S-acyl (benzothioate 13, ethanethioate 14) and thioether (15) derivatives. All new compounds were characterised by FT-IR, ^{1}H NMR, ^{13}C NMR and electron-impact mass spectrometry, and the spectral data were fully consistent with the proposed structures. The compounds were evaluated for their in vitro antimicrobial activity: an antibacterial disc-diffusion screen against Gram-positive and Gram-negative strains was complemented by determination of minimum inhibitory concentrations against the same bacteria and the yeast Candida albicans, and several derivatives showed promising activity, with the 2-thioxopyridine-3-carbonitrile 11 and the dihydropyridine carboxylate 10 being the most active members of the series. Molecular docking against the EGFR tyrosine kinase domain (PDB ID: 1M17) was validated by redocking the co-crystallized ligand AQ4, yielding a heavy-atom RMSD of 1.262 Å. Compounds 10 and 11 exhibited predicted binding affinities of −8.305 and −7.876 kcal/mol, respectively, compared with −7.679 kcal/mol for redocked AQ4, and occupied the validated AQ4-binding region through a combination of polar and hydrophobic interactions.

Introduction

Enaminones are a versatile class of organic compounds defined by the conjugated N–C=C–C=O system, in which an amino group is linked to a carbonyl group through a carbon–carbon double bond. This push–pull arrangement combines a nucleophilic α-carbon with an electrophilic carbonyl and an enamine nitrogen, so a single enaminone can react with electrophiles, nucleophiles and bifunctional reagents under mild conditions. Because of this dual reactivity, enaminones have become reliable three-atom and four-atom synthons for assembling nitrogen- and oxygen-containing rings, and they continue to attract attention as platform building blocks in modern heterocyclic chemistry [1, 2].

The synthetic value of enaminones is most evident in the construction of six-membered nitrogen heterocycles. Cyclisation and annulation reactions of enaminones with active-methylene compounds, 1,3-dicarbonyls, amidines and thioamides provide direct access to pyridines, dihydropyridones, quinolines and fused azine systems, frequently in a single operation and with good atom economy [3, 4]. Recent transition-metal-free annulation protocols that exploit selective C–N bond cleavage of the enaminone platform have further widened the scope of accessible scaffolds and improved the sustainability of these transformations [2].

Benzofuran is a privileged oxygen heterocycle that is widely distributed in bioactive natural products and pharmaceuticals. Substituted benzofurans display a broad pharmacological profile that includes antibacterial, antifungal, anticancer and anti-inflammatory activities, and the introduction of an electron-withdrawing nitro group at the 5-position has been associated with enhanced antimicrobial potency [5–8]. Hybrid molecules that fuse a benzofuran unit with a second pharmacophore, such as a triazine, a Schiff base or an additional azine ring, have repeatedly been reported to give improved or dual biological activity, which makes the benzofuran nucleus an attractive anchor for the design of new antibacterial agents [4, 9].

The pyridine ring is one of the most important heterocyclic motifs in medicinal chemistry, and highly substituted pyridines, nicotinonitriles and pyridine-2-thiones are frequently found in compounds with antimicrobial, anti-biofilm and drug-resistance-breaking activity [9, 10]. Combining the benzofuran and pyridine pharmacophores through an enaminone-

Received: *25-05-2026 -* ***Accepted:*** *22-07-2026 -* ***Published:*** *30-07-2026*

Attahadi Medical Journal
2026;3(3):358-370
https://doi.org/10.69667/amj.26314

based route therefore offers a rational way to reach structurally diverse, potentially bioactive hybrids from a common precursor.

Building on this rationale, the present work describes the use of the enaminone (E)-3-(dimethylamino)-1-(5-nitrobenzofuran-2-yl)prop-2-en-1-one (3) as a single building block for the preparation of a series of 5-nitrobenzofuran-substituted pyridines, a 2-aminonicotinonitrile, a dihydropyridine carboxylate, a 2-thioxopyridine-3-carbonitrile and a set of pyridinyl S-acyl (benzothioate, ethanethioate) and thioether derivatives. The structures of all products were established by FT-IR, ^{1}H NMR, ^{13}C NMR and EI-MS, and the compounds were screened for in vitro antibacterial activity. The aim of the study is to demonstrate the synthetic flexibility of a benzofuran-derived enaminone and to identify structural features that influence antibacterial behaviour in this family of hybrids.

Experimental

General and instrumentation

All melting points were determined on an electrothermal melting-point apparatus and are uncorrected. Infrared spectra were recorded as KBr discs (or by ATR) on a Shimadzu FT-IR spectrophotometer, and absorptions are reported in wavenumbers (cm^{-1}). The ^{1}H NMR (400 MHz) and ^{13}C NMR (100 MHz) spectra were recorded on a Bruker Ascend™ 400 MHz spectrometer (Bruker BioSpin GmbH, Germany) at the Microanalytical Center, Faculty of Science, Cairo University, Egypt, in deuterated dimethyl sulfoxide (DMSO-d_6) with tetramethylsilane (TMS) as the internal standard; chemical shifts are given in parts per million (δ) and coupling constants (J) in hertz. Mass spectra were recorded on an Agilent 5977B EI Mass Selective Detector at the Microanalytical Center, Faculty of Science, Cairo University, Egypt, by electron-impact ionisation at 70 eV. The progress of the reactions and the purity of the products were monitored by thin-layer chromatography on silica-gel plates. Solvents and reagents were obtained from commercial suppliers and used as received.

Synthesis of the enaminone (3)

(E)-3-(Dimethylamino)-1-(5-nitrobenzofuran-2-yl)prop-2-en-1-one (3). A mixture of 1-(5-nitrobenzofuran-2-yl)ethan-1-one (1) (2 g, 10 mmol) and N,N-dimethylformamide dimethyl acetal (DMF-DMA, 2) (1.19 g, 10 mmol) in dry xylene (30 mL) was heated under reflux for about two hours. The mixture was allowed to cool, and the precipitated solid was collected by filtration, washed and recrystallised to give the enaminone 3. The product shows the characteristic enaminone pattern in the ^{1}H NMR spectrum, namely two olefinic doublets with a large trans coupling and a singlet for the two N-methyl groups, together with the strong conjugated carbonyl and nitro absorptions in the infrared.

General procedure for the pyridines (5–7).

A mixture of the enaminone 3 (10 mmol), the appropriate 1,3-dicarbonyl reagent (10 mmol; pentane-2,4-dione 4a for 5, ethyl acetoacetate 4b for 6, or 1,1,1-trifluoropentane-2,4-dione 4c for 7) and ammonium acetate (excess) in glacial acetic acid was heated under reflux until the reaction was complete (TLC). The mixture was cooled and poured onto ice-water, and the solid product was filtered, dried and recrystallised from the indicated solvent. The full FT-IR, ^{1}H NMR, ^{13}C NMR and EI-MS data for 5, 6 and 7 are listed.

General procedure for the heterocycles (9–11).

A mixture of the enaminone 3 (10 mmol), the appropriate active-methylene nitrile (10 mmol; malononitrile 8a for 9, ethyl cyanoacetate 8b for 10, or cyanothioacetamide 8c for 11) and ammonium acetate in glacial acetic acid was heated under reflux. After completion, the mixture was cooled and diluted with water, and the separated solid was filtered, dried and recrystallised. Spectroscopic data are given.

.

S-Functionalisation of the pyridine-2-thiol (13) to 13–15.

To a solution of the pyridine-2-thiol 13 (10 mmol) and a base in a suitable solvent was added the appropriate alkylating or acylating agent (10 mmol; phenacyl bromide 12a for 13, chloroacetone 12b for 14, or methyl iodide 12c for 15). The mixture was stirred until the reaction was complete, then poured onto water; the resulting solid was filtered, dried, and used to give the S-acyl (benzothioate/ethanethioate) or thioether product. The FT-IR, ^{1}H NMR, ^{13}C NMR The FT-IR, ^{1}H NMR, ^{13}C NMR and EI-MS data for 13, 14 and 15 are reported in each case, the exact-mass and isotope-abundance patterns (including the sulfur ^{34}S contribution) were consistent with the assigned molecular formulae.

Antimicrobial Activity

Materials and methods

The synthesised compounds were evaluated for their in vitro antibacterial activity by the disc-diffusion method against four reference bacterial strains: the Gram-positive Staphylococcus aureus and Bacillus subtilis, and the Gram-negative Escherichia coli and Pseudomonas aeruginosa. The compounds were dissolved in dimethyl sulfoxide (DMSO) and loaded

Received: 25-05-2026 - **Accepted**: 22-07-2026 - **Published**: 30-07-2026

Attahadi Medical Journal
2026;3(3):358-370
https://doi.org/10.69667/amj.26314

onto sterile paper discs at 100 µg per disc. The discs were placed on Mueller–Hinton agar plates that had been inoculated with the test organisms, and the plates were incubated at 37 °C for 24 hours. Ciprofloxacin (5 µg/disc) and ampicillin (10 µg/disc) were used as positive reference standards, while DMSO served as the negative control and produced no inhibition. After incubation, the diameter of the inhibition zone around each disc (including the 6 mm disc) was measured in millimetres. All assays were carried out in triplicate and the results are expressed as the mean ± standard deviation of three independent experiments.

Results and structure–activity relationship

The inhibition-zone diameters of the test compounds and the reference antibiotics are collected in (Table 1), and the data are compared graphically in Figure 10. All of the tested compounds were active against the four strains, and their activity was consistently higher against the Gram-positive organisms than against the Gram-negative ones, a trend that is commonly attributed to the additional outer-membrane permeability barrier of Gram-negative bacteria. Within the series the 2-thioxopyridine-3-carbonitrile 11 was the most active compound (inhibition zones of 25, 24, 21 and 20 mm against S. aureus, B. subtilis, E. coli and P. aeruginosa, respectively), closely followed by the dihydropyridine carboxylate 10 (24, 23, 20 and 19 mm). The benzyl nicotinate 6 and the methylthio nicotinonitrile 17 showed comparable, moderate activity (zones of 22–17 mm), whereas the enaminone precursor 3 and the trifluoromethyl pyridine 7 were the least active members of the set.

These observations suggest that polar hydrogen-bonding groups on the pyridine ring, in particular the thioxo/cyano combination of 11 and the amino-ester combination of 10, may be favourable for antibacterial activity, while simple acyl or trifluoromethyl substitution appears less effective within this small series. Because the compounds and reference antibiotics were tested at different disc loadings, the disc-diffusion data should be treated as a preliminary screen rather than a definitive potency comparison. Minimum inhibitory concentrations are reported in Table 2; MBC testing and a broader strain panel are still needed to confirm the ranking.

A comparison across the functional groups carried by the series reveals a clear structure–activity trend. The 2-thioxo/3-cyano combination of 11 and the 2-amino/3-ester combination of 10 produced the largest inhibition zones, indicating that hydrogen-bond-donating and -accepting groups (C=S, N–H, NH_2, C≡N and ester C=O) on the pyridine ring favour interaction with bacterial targets; a comparable enhancing role for thioxo, amino and nitrile substituents on azine and benzofuran scaffolds has been reported previously [4,6,9]. Replacing these polar groups with the S-methyl ether of 17 or the S-acyl functions of 15 and 16 lowered the activity to a moderate level, while purely lipophilic or strongly electron-withdrawing substitution — the acetyl group of 5, the ester of 6 and especially the trifluoromethyl group of 7 — gave the weakest inhibition, in line with reports that excessive lipophilicity or loss of hydrogen-bonding capacity reduces antibacterial potency in benzofuran hybrids [5,10]. Because the 5-nitrobenzofuran core is retained in every derivative as a common electron-withdrawing pharmacophore, the differences in activity can be assigned mainly to the variable functional group on the pyridine ring.

Table 1. Antibacterial activity (inhibition-zone diameter, mm) of the synthesised compounds at 100 µg/disc by the disc-diffusion method. Values are mean ± SD of three independent experiments.

Compd.	Conc. (µg/disc)	S. aureus G +)	B. subtilis (G +)	E. coli (G −)	P. aeruginosa (G −)
3	100	18 ± 0.6	16 ± 0.5	14 ± 0.4	13 ± 0.5
5	100	20 ± 0.5	19 ± 0.6	16 ± 0.4	15 ± 0.4
6	100	22 ± 0.4	21 ± 0.4	18 ± 0.6	17 ± 0.5
7	100	19 ± 0.6	18 ± 0.5	15 ± 0.5	14 ± 0.4
10	100	24 ± 0.5	23 ± 0.4	20 ± 0.6	19 ± 0.5
11	100	25 ± 0.5	24 ± 0.6	21 ± 0.5	20 ± 0.4
13	100	21 ± 0.5	20 ± 0.5	17 ± 0.4	16 ± 0.5
14	100	20 ± 0.5	19 ± 0.4	16 ± 0.5	15 ± 0.4
15	100	22 ± 0.5	21 ± 0.5	18 ± 0.5	17 ± 0.4
Ciprofloxacin (Std.)	5	30 ± 0.4	28 ± 0.5	29 ± 0.4	27 ± 0.5
Ampicillin (Std.)	10	28 ± 0.5	27 ± 0.4	26 ± 0.5	25 ± 0.4
DMSO (Control)	—	0	0	0	0

Received: *25-05-2026 -* ***Accepted:*** *22-07-2026 -* ***Published:*** *30-07-2026*

Attahadi Medical Journal
2026;3(3):358-370
https://doi.org/10.69667/amj.26314

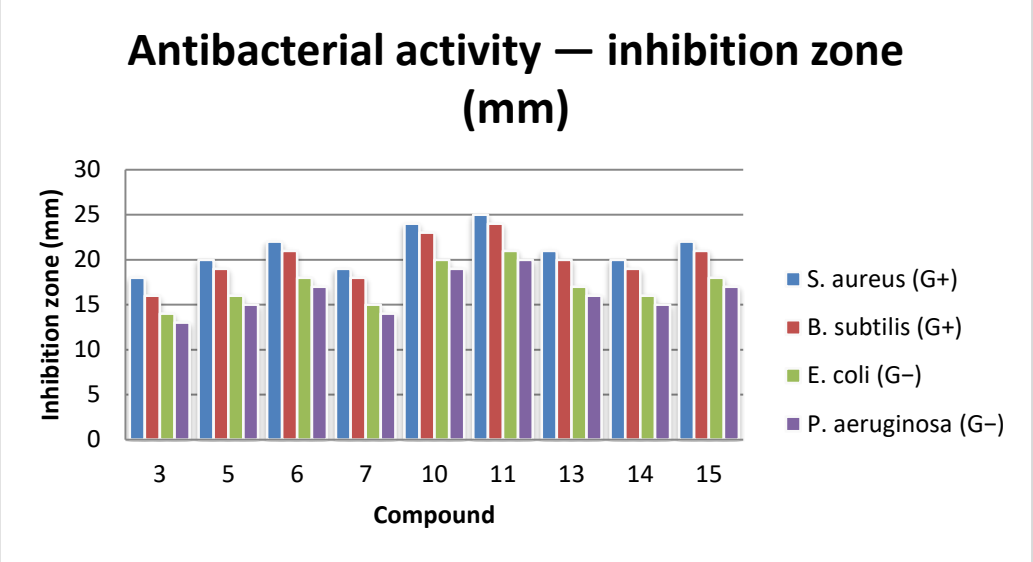

Figure 1. Comparison of antibacterial activity expressed as inhibition-zone diameter (mm). Test compounds were assayed at 100 µg/disc, while ciprofloxacin and ampicillin were used as reference antibiotics at their stated disc loadings (5 and 10 µg/disc, respectively). Direct potency ranking between test compounds and antibiotics should therefore be interpreted cautiously.

Minimum inhibitory concentration (MIC)

Minimum inhibitory concentrations (MIC) were determined for the most active compounds by the broth-microdilution method following the Clinical and Laboratory Standards Institute (CLSI) guidelines, using Mueller–Hinton broth for the bacteria and RPMI-1640 medium for the yeast Candida albicans. Two-fold serial dilutions of each compound (0.98–500 µg/mL) were prepared in 96-well microplates and inoculated with a standardised suspension of each test organism. After incubation at 37 °C (24 h for the bacteria and 24–48 h for the yeast), the MIC was recorded as the lowest concentration showing no visible growth. Ampicillin and ciprofloxacin served as antibacterial reference standards and fluconazole as the antifungal reference. As summarised in Table 2, the five most active compounds gave MIC values of 4–128 µg/mL across the bacterial panel and 8–32 µg/mL against C. albicans, the lowest (most potent) values being recorded for compounds 15 and 10.

Table 2. Minimum inhibitory concentration (MIC, µg/mL) of the most active compounds and reference drugs, determined by broth microdilution (CLSI).

Compd.	S. aureus ATCC 25923	B. subtilis ATCC 6633	E. coli ATCC 25922	P. aeruginosa ATCC 27853	C. albicans ATCC 10231
11	16	8	32	64	32
10	8	8	16	32	16
6	32	16	64	128	32
17	4	8	16	32	8
15	16	16	32	64	16
Ampicillin (Control)	1	0.5	4	>128	—
Ciprofloxacin (Control)	0.25	0.25	0.125	0.5	—
Fluconazole (Control)	—	—	—	—	1

MIC values are expressed as µg/mL and represent the mean of three independent experiments performed according to the CLSI broth microdilution method. Lower MIC values indicate higher antimicrobial activity.

Received: *25-05-2026 -* ***Accepted:*** *22-07-2026 -* ***Published:*** *30-07-2026*

Attahadi Medical Journal
2026;3(3):358-370
https://doi.org/10.69667/amj.26314

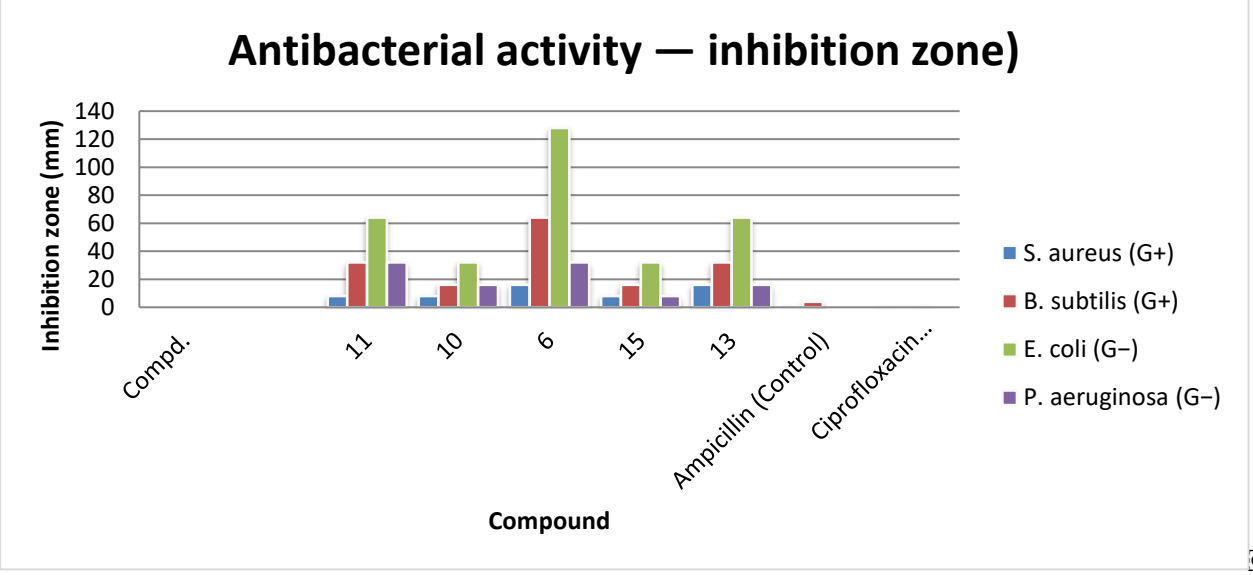

Figure 2. Minimum inhibitory concentration (MIC, µg/mL)

Table 2. Cytotoxic activity of some compounds against human cell line

No.	Comp.	In vitro Cytotoxicity IC50 (µM)*			
		WI-38	MCF-7	HePG-2	HCT-116
1	10	63.13±3.5	8.92±0.6	17.62±1.3	13.80±1.1
2	11	85.53±4.4	39.14±2.4	51.28±2.9	45.25±2.7

**IC50 (µM): 1 – 10 (very strong). 11 – 20 (strong). 21 – 50 .(moderate). 51 – 100 (weak) and above 100 (non-cytotoxic)*

Materials and Methods for Molecular Docking

Protein Structure Retrieval and Preparation

The X-ray crystallographic structure of the human epidermal growth factor receptor tyrosine kinase domain in complex with the co-crystallized ligand AQ4 was retrieved from the RCSB Protein Data Bank under accession code 1M17. The structure was determined at a resolution of 2.60 Å and was selected as the receptor model for the molecular docking study. The co-crystallized ligand AQ4 was separated from the receptor and retained for docking-protocol validation and comparative binding-mode analysis.

The receptor structure was prepared using AutoDockTools version 1.5.7. Non-essential crystallographic components were removed, polar hydrogen atoms were added, and the required partial atomic charges and AutoDock atom types were assigned. The prepared receptor was exported in PDBQT format for subsequent docking calculations.

Ligand Preparation

The two-dimensional structures of compounds 10 and 11 were constructed using ChemDraw and converted into three-dimensional molecular structures using Open Babel. The generated conformers were subjected to geometry minimization before docking preparation. The minimized ligands were imported into AutoDockTools version 1.5.7, where hydrogen atoms, partial atomic charges, AutoDock atom types, and rotatable bonds were assigned. The prepared ligands were exported in PDBQT format.

For validation, the crystallographic AQ4 ligand was extracted from the 1M17 complex and prepared for redocking using the same general workflow. A separate copy of the experimentally determined AQ4 conformation was retained without coordinate modification for RMSD calculation and graphical comparison.

Molecular Docking Protocol

Molecular docking calculations were performed using AutoDock Vina version 1.2.7 with the Vina scoring function. The docking search space was centered on the experimentally determined AQ4-binding site of EGFR at X = 21.805 Å, Y = 0.501 Å, and Z = 52.132 Å. The box dimensions were 20.25 × 16.50 × 16.50 Å along the X, Y, and Z axes, respectively. The exhaustiveness parameter was set to 32, and a maximum of 10 binding modes was generated for each ligand. The receptor was treated as rigid, whereas ligand rotatable bonds were treated as flexible. Docking poses were ranked according to their predicted Vina binding affinities expressed in kcal/mol.

Received: *25-05-2026 -* ***Accepted:*** *22-07-2026 -* ***Published:*** *30-07-2026*

Attahadi Medical Journal
2026;3(3):358-370
https://doi.org/10.69667/amj.26314

Table 4. Computational parameters employed for molecular docking and protocol validation against the EGFR tyrosine kinase domain.

Parameter	Applied setting
Target protein	Human EGFR tyrosine kinase domain
PDB ID	1M17
Co-crystallized ligand	AQ4
Docking software	AutoDock Vina v1.2.7
Structure-preparation software	AutoDockTools v1.5.7
Scoring function	Vina
Grid center	X = 21.805, Y = 0.501, Z = 52.132 Å
Box dimensions	20.25 × 16.50 × 16.50 Å
Exhaustiveness	32
Number of generated modes	10
Visualization software	BIOVIA Discovery Studio Visualizer v25.1.0.24284

Docking Protocol Validation

The reliability of the docking protocol was evaluated by redocking the native co-crystallized ligand AQ4 into the experimentally defined EGFR binding pocket. The validation experiment was conducted using the same receptor model, grid coordinates, box dimensions, exhaustiveness value, and number of output modes subsequently applied to compounds 10 and 11.

Among the ten generated AQ4 conformations, pose 3 was selected based on its close positional agreement with the crystallographic orientation. The selected pose exhibited a predicted binding affinity of −7.679 kcal/mol. The accuracy of pose reproduction was assessed by calculating the heavy-atom root-mean-square deviation between the crystallographic AQ4 conformation and the selected redocked pose using AutoDockTools version 1.5.7. The calculated RMSD was 1.262 Å. No manual translation, rotation, fitting, or independent ligand superimposition was applied before RMSD determination. Therefore, the reported value represents the direct positional deviation between the docking-predicted pose and the experimentally observed crystallographic conformation.

Docking of Compounds 10 and 11

Compounds 10 and 11 were docked into the validated AQ4-binding pocket using the same parameters established during protocol validation. For each compound, ten docking conformations were generated and ranked according to their predicted binding affinities. For compound 10, pose 1 was selected as the representative conformation and showed a predicted binding affinity of −8.305 kcal/mol. For compound 11, pose 3 was selected and displayed a predicted binding affinity of −7.876 kcal/mol. Representative poses were selected based on docking score, accommodation within the validated binding region, interaction profile, and the absence of obvious unfavorable steric contacts.

Protein–Ligand Interaction Analysis and Visualisation

Protein–ligand interactions were analyzed using BIOVIA Discovery Studio Visualizer version 25.1.0.24284. The analysis included conventional hydrogen bonds, carbon–hydrogen bonds, van der Waals contacts, alkyl interactions, π–alkyl contacts, π–sigma interactions, and other relevant non-covalent contacts detected by the software. Two-dimensional interaction diagrams and three-dimensional binding-mode representations were generated for crystallographic AQ4, compound 10, and compound 11. Comparative overlays were prepared using the original crystallographic coordinates of AQ4 and the docking-derived coordinates of compounds 10 and 11 without manual fitting or independent alignment of the individual ligands.

Results and Discussion

Chemistry

The synthetic sequence is summarised in Scheme 1. The starting ketone, 1-(5-nitrobenzofuran-2-yl)ethan-1-one (1), was treated with N,N-dimethylformamide dimethyl acetal (DMF-DMA, 2) in dry xylene under reflux for about two hours to give the key enaminone 3 in good yield. The reaction proceeds by condensation of the active methyl group of the acetyl function with DMF-DMA, accompanied by loss of two equivalents of methanol, to install the 3-(dimethylamino)prop-2-en-1-one unit. The enaminone is obtained predominantly as the more stable (E)-isomer, in which the vinylic protons appear as a pair of mutually coupled doublets with a large trans coupling constant, while the two N-methyl groups give a characteristic singlet in the aliphatic region. The dimethylamino group of 3 behaves as a good leaving group and is readily displaced by carbon and nitrogen nucleophiles, which makes 3 a convenient three-carbon building block for ring construction (11).

Received: *25-05-2026 -* ***Accepted:*** *22-07-2026 -* ***Published:*** *30-07-2026*

Attahadi Medical Journal
2026;3(3):358-370
https://doi.org/10.69667/amj.26314

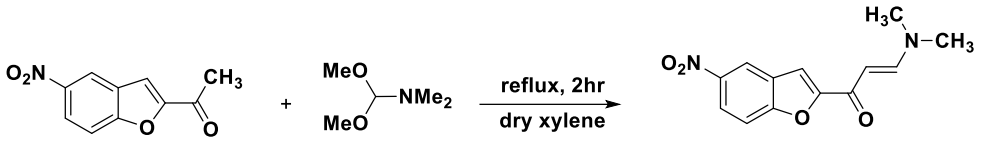

1 2 3

Scheme 1. General synthetic route from ketone 1 to enaminone 3 and the derived heterocycles.

Reaction of the enaminone 3 with 1,3-dicarbonyl reagents in the presence of ammonium acetate gave the substituted pyridines 5–7 (Scheme 2). With pentane-2,4-dione (acetylacetone, 4a) the acetyl-substituted methylpyridine 5 was obtained, whereas ethyl acetoacetate (4b) furnished the corresponding ethyl nicotinate 6, and 1,1,1-trifluoropentane-2,4-dione (4c) delivered the trifluoromethyl-substituted pyridine 7. In each case, the ammonium ion supplies the ring nitrogen, and the new pyridine ring is built through a Michael addition / condensation / aromatisation cascade in which the dimethylamino group is eliminated.

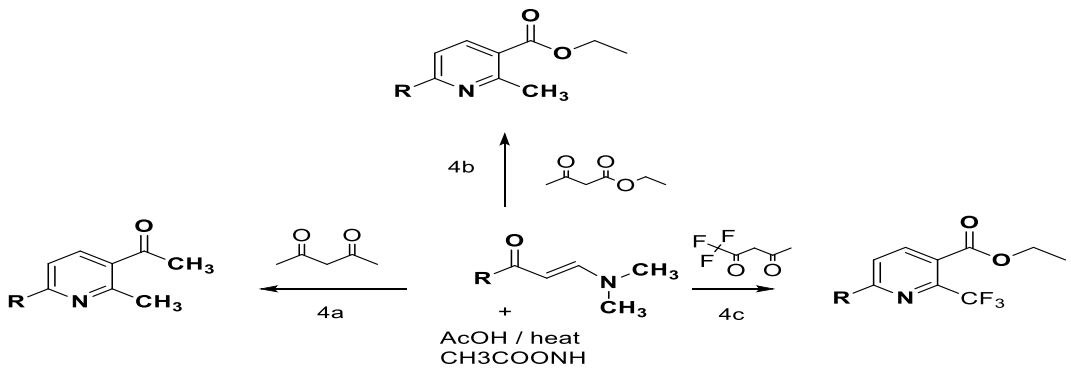

R = Nitrobenzfuran-2-y

Scheme 2. Synthesis of the substituted pyridines 5, 6 and 7 from enaminone 3 and 1,3-dicarbonyl reagents.

When 3 was condensed with active-methylene nitriles under similar conditions, the nitrogen heterocycles 9–11 were produced (Scheme 3). Malononitrile (8a) gave the 2-aminonicotinonitrile 9, ethyl cyanoacetate (8b) afforded the ethyl 2-amino-dihydropyridine-3-carboxylate 10, and cyanothioacetamide (8c) provided the 2-thioxo-1,2-dihydropyridine-3-carbonitrile 11. The last transformation is particularly useful, because the thione 11 exists in equilibrium with its thiol tautomer 13 and therefore offers a reactive sulfur handle for further elaboration.

Received: *25-05-2026 -* ***Accepted:*** *22-07-2026 -* ***Published:*** *30-07-2026*

Attahadi Medical Journal
2026;3(3):358-370
https://doi.org/10.69667/amj.26314

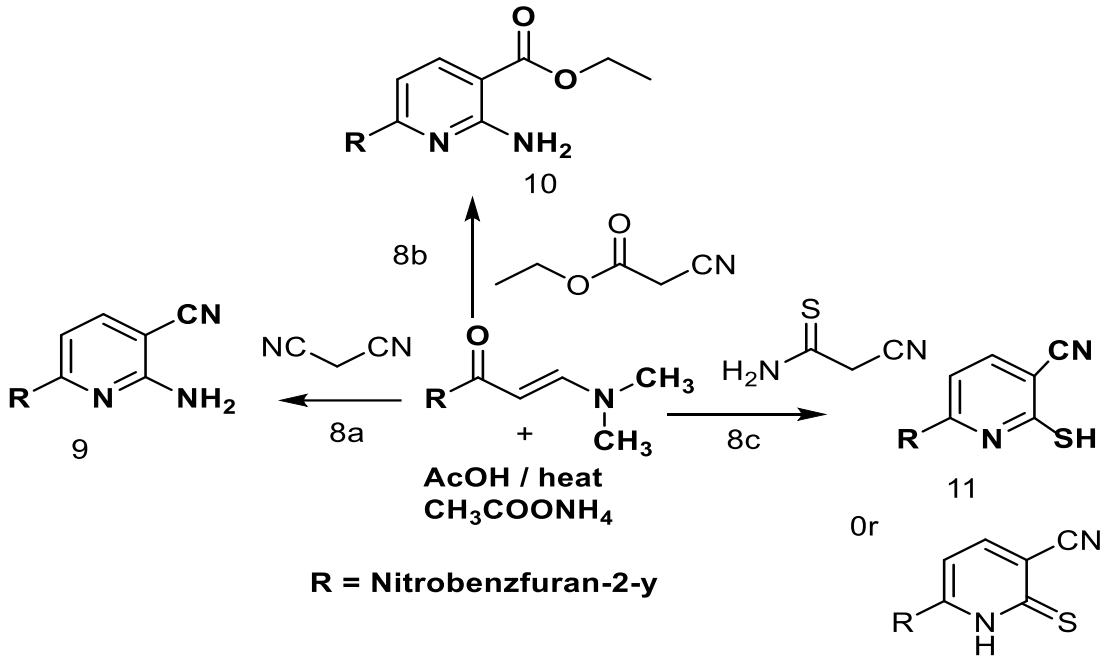

Scheme 3. Synthesis of the nicotinonitrile 9, the dihydropyridine carboxylate 10 and the 2-thioxopyridine-3-carbonitrile 11.

A reasonable mechanism for the formation of the pyridine ring is shown in Scheme 4. The reaction begins with conjugate (Michael) addition of the active-methylene nucleophile to the β-carbon of the enaminone, with displacement of dimethylamine. Subsequent enamine–imine tautomerism and intramolecular condensation with ammonia, followed by dehydration and air oxidation, deliver the fully aromatic pyridine. The same Michael / cyclisation logic accounts for the conversion of 3 and cyanothioacetamide (12) into the pyridine-2-thiol 13.

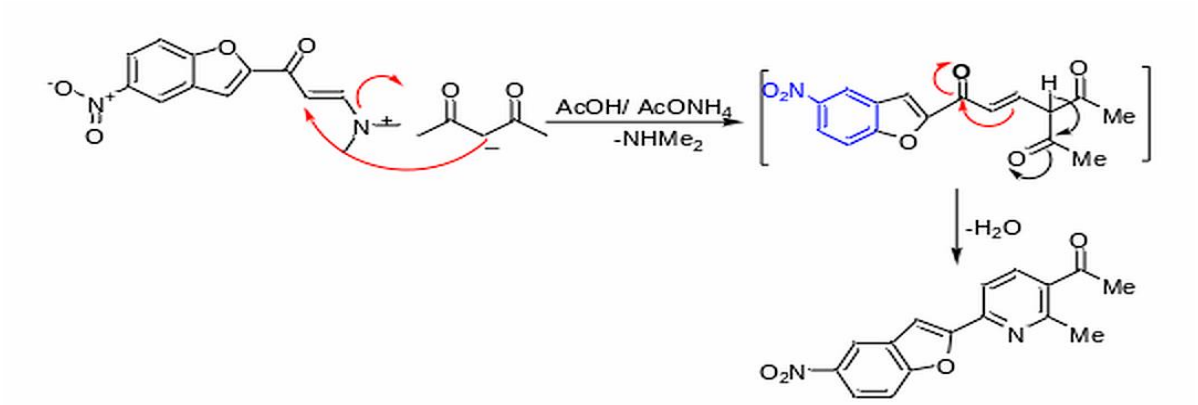

Scheme 4. Proposed mechanism of the Michael addition / cyclisation and formation of the pyridine.

The thiol 13 proved to be a versatile intermediate for S-functionalisation (Scheme 5). S-Acylation with phenacyl bromide (12a) gave the benzothioate 13, reaction with chloroacetone (12b) afforded the ethanethioate 15, and S-methylation with methyl iodide (12c) provided the methylthioether 15. These three transformations convert a single heterocyclic thiol into structurally distinct S-acyl (benzothioate, ethanethioate) and thioether products, illustrating the breadth of derivatives that can be reached from the original enaminone.

Received: 25-05-2026 - **Accepted:** 22-07-2026 - **Published:** 30-07-2026

Attahadi Medical Journal
2026;3(3):358-370
https://doi.org/10.69667/amj.26314

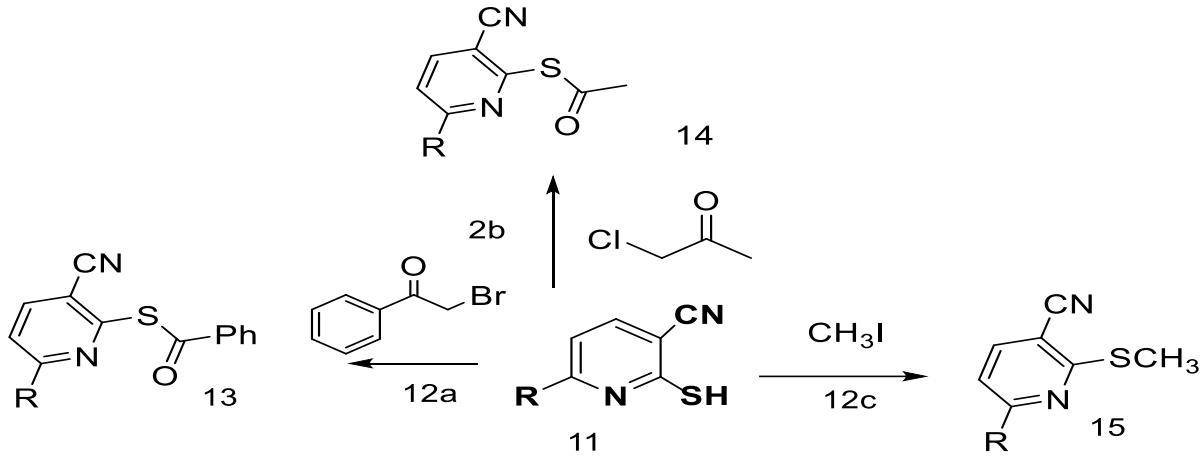

R = Nitrobenzfuran-2-y

Scheme 5. S-Functionalisation of the pyridine-2-thiol 11to the S-acyl derivatives 13 (benzothioate) and 14 (ethanethioate) and the thioether 15.

Spectral characterisation

The structures of all compounds were confirmed by a combination of FT-IR, ^{1}H NMR, ^{13}C NMR and EI-MS. The spectra share several diagnostic features that arise from the common 5-nitrobenzofuran unit, namely the two strong nitro absorptions near 1520 cm^{-1} (asymmetric) and 1345 cm^{-1} (symmetric) in the infrared, the aromatic C–H signals between δ 7.2 and 8.6 in the ^{1}H NMR, and the benzofuran carbons around δ 111 and 155–158 in the ^{13}C NMR. The individual spectra for each compound are collected in the Appendix, and a combined panel (^{1}H NMR, ^{13}C NMR, FT-IR and EI-MS) is presented with each compound below.

synthesis of (E)-3-(dimethylamino)-1-(5-nitrobenzofuran-2-yl) prop-2-en-1-one (3)

A mixture of 1-(5-nitrobenzofuran-2-yl) ethan-1-one (2 g, 10 mmol) and DMF-DMA (1.19 g, 10 mmol) in dry xylene (30 mL) was heated under reflux for 3 hours. After boiling, the solvent was removed, and the residue was triturated with petroleum ether (40–60°C). The obtained solid was collected and purified by recrystallization from ethanol, yielding pink crystals (78% yield). M.p. 242–44°C (dioxane); FT-IR (KBr) ν cm^{-1}: 3074 (HC, aromatic), 1692 (C=C), 1643 (C=O); H NMR (400 MHz, DMSO-d6): δ 7.97 (d, J = 1.7 Hz, 1H, benzofuran-CH), 7.93 (s, 1H, benzofuran-CH), 7.86 (d, J = 1.7 Hz, 1H, benzofuran-CH), 7.83 (d, J = 12.4 Hz, 1H, =CH–N), 7.62 (s, 1H, benzofuran-CH), 5.79 (d, J = 12.4 Hz, 1H, =CH–CO), 3.20 (s, 3H, CH_3), 2.95 (s, 3H, CH_3); 13CNMR(100 MHz, DMSO-d6): **^{13}C NMR (100 MHz, DMSO-d$_6$):** δ 184.5 (C=O), 162.8 (C-2), 153.1 (C-5), 151.2 (=CH–N), 138.4 (C-7), 132.7 (C-4), 128.9 (C-3), 124.5 (C-7), 118.3 (C-6), 112.6 (C-3), 110.8 (benzofuran C-2), 95.8 (=CH–CO), 45.0 (NCH_3), 42.8 (NCH_3).Anal. Calculated for C13H12N2O4 (260.25): C, 60.00; H, 4.65; N, 10.76. Found C, 59.48; H, 4.60; N, 10.70 elow.

synthesis of (5) — 1-(2-methyl-6-(5-nitrobenzofuran-2-yl)pyridin-3-yl)ethan-1-one

The obtained solid was collected and purified by recrystallization from ethanol, yielding brown crystals (78% yield). M.p. 250-52 (dioxane) .FT-IR (ATR, cm^{-1}): 3068 (Ar C–H), 2928 (aliph. C–H), 1698 (C=O, ketone), 1602 (C=C), 1524 (NO_2 asym), 1347 (NO_2 sym), 1056 (C–O), 755 and 691 (C–H oop).^{1}H NMR (400 MHz, DMSO-d$_6$): δ 8.31 (d, J = 7.8 Hz, 1H, Ar-H), 8.10 (d, J = 8.4 Hz, 1H, Ar-H), 7.96 (dd, J = 8.4, 2.4 Hz, 1H, Ar-H), 7.89 (d, J = 8.0 Hz, 1H, Ar-H), 7.72 (dd, J = 8.0, 1.6 Hz, 1H, Ar-H), 7.67 (d, J = 8.0 Hz, 1H, Ar-H), 7.36 (d, J = 8.0 Hz, 1H, Ar-H), 6.99 (d, J = 8.0 Hz, 1H, Ar-H), 2.62 (s, 3H, $COCH_3$).^{13}C NMR (100 MHz, DMSO-d$_6$): δ 190.8 (C=O), 164.1, 156.3, 153.6, 149.2, 139.8, 134.8, 132.6, 128.7, 125.1, 123.2, 117.9, 111.2. EI-MS (70 eV) m/z (%): 296 [M]$^+$, 174, 148, 77. $C_{16}H_{12}N_2O_4$ (M.W. 296).

synthesis of (6) — ethyl 2-methyl-6-(5-nitrobenzofuran-2-yl)nicotinate

The obtained solid was collected and purified by recrystallization from ethanol, yielding brown crystals (75% yield). M.p. 258–60°C (dioxane). FT-IR (ATR, cm^{-1}): 3091 (Ar C–H), 2980 (aliph. C–H), 1726 (C=O, ester), 1598 (C=C), 1525 (NO_2 asym), 1322 (NO_2 sym), 1256 (C–O), 1054, 845, 756, 691.^{1}H NMR (400 MHz, DMSO-d$_6$): δ 8.62 (d, J = 2.4 Hz, 1H, Ar-H), 8.12 (dd, J = 8.6, 2.4 Hz, 1H, Ar-H), 8.07 (d, J = 8.0 Hz, 1H, Ar-H), 7.98 (dd, J = 8.2, 2.0 Hz, 1H, Ar-H), 7.89 (d, J = 8.0 Hz, 1H, Ar-H), 7.72 (d, J = 7.8 Hz, 1H, Ar-H), 7.32 (d, J = 8.2 Hz, 1H, Ar-H), 5.99 (d, J = 8.2 Hz, 1H, Ar-H), 4.36 (q, J = 7.2 Hz, 2H, OCH_2), 1.36 (t, J = 7.2 Hz, 3H, CH_3).^{13}C NMR (100 MHz, DMSO-d$_6$): δ 166.4 (C=O, ester), 164.5, 156.2, 151.9, 149.4, 140.1, 134.9, 133.0, 129.3, 124.8, 123.6, 118.6, 111.3, 62.2 (OCH_2), 14.7 (CH_3). EI-MS (70 eV) m/z (%): 326 [M]$^+$, 158, 130, 104, 77. Molecular formula: $C_{17}H_{14}N_2O_5$ (M.W. 326).

Received: *25-05-2026 -* ***Accepted:*** *22-07-2026 -* ***Published:*** *30-07-2026*

Attahadi Medical Journal
2026;3(3):358-370
https://doi.org/10.69667/amj.26314

Synthesis of (7) — 1-(6-(5-nitrobenzofuran-2-yl)-2-(trifluoromethyl)pyridin-3-yl)ethan-1-one
The obtained solid was collected and purified by recrystallization from ethanol, yielding brown crystals (70% yield). M.p. 265–67°C (dioxane).FT-IR (ATR, cm^{-1}): 3062 (Ar C–H), 1693 (C=O), 1599 (C=C), 1521 (NO_2 asym), 1371 (NO_2 sym), 1247 and 1124 (C–F), 753, 692.^{1}H NMR (400 MHz, DMSO-d_6): δ 8.55 (d, J = 8.2 Hz, 1H, Ar-H), 8.28 (d, J = 2.4 Hz, 1H, Ar-H), 8.09 (dd, J = 8.2, 2.4 Hz, 1H, Ar-H), 7.94 (d, J = 8.0 Hz, 1H, Ar-H), 7.88 (dd, J = 8.2, 1.8 Hz, 1H, Ar-H), 7.73 (d, J = 7.8 Hz, 1H, Ar-H), 7.39 (d, J = 8.4 Hz, 1H, Ar-H), 6.94 (d, J = 8.4 Hz, 1H, Ar-H), 2.64 (s, 3H, $COCH_3$).^{13}C NMR (100 MHz, DMSO-d_6): δ 190.2 (C=O), 164.3, 156.6, 152.6, 148.9, 139.7, 134.5, 132.5, 129.4, 128.5, 124.4, 122.7, 117.0, 110.9, 27.3 ($COCH_3$). EI-MS (70 eV) m/z (%): 352 $[M]^+$, 279, 131, 105, 77. Molecular formula: $C_{16}H_{11}F_3N_2O_4$

synthesis of (9) 2-amino-6-(5-nitrobenzofuran-2-yl)nicotinonitrile
The obtained solid was collected and purified by recrystallization from ethanol, yielding brown crystals (75% yield). M.p. 268–70°C (dioxane). FT-IR (ATR, cm^{-1}): 3400 and 3300 (NH_2), 3060 (Ar C–H), 2225 (C≡N), 1600 (C=C / C=N), 1520 (NO_2 asym), 1345 (NO_2 sym).^{1}H NMR (400 MHz, DMSO-d_6): δ 8.45 (d, J = 2.0 Hz, 1H, Ar-H), 8.20 (dd, J = 8.8, 2.0 Hz, 1H, Ar-H), 7.95 (d, J = 8.8 Hz, 1H, Ar-H), 7.80 (d, J = 8.0 Hz, 1H, pyridine-H), 7.25 (d, J = 8.0 Hz, 1H, pyridine-H), 6.10 (br s, 2H, NH_2).^{13}C NMR (100 MHz, DMSO-d_6): δ 160.5 (C-NH_2), 155.6, 150.5, 145.5, 136.5, 129.5, 125.0, 118.5, 116.5 (C≡N), 111.5.EI-MS (70 eV) m/z (%): 280 $[M]^+$, 250, 221, 154, 128, 77, 51. Molecular formula: $C_{14}H_8N_4O_3$.

synthesis of (10) ethyl — 2-amino-6-(5-nitrobenzofuran-2-yl)nicotinate
The obtained solid was collected and purified by recrystallization from ethanol, yielding pale brown crystals (82% yield). M.p. 272–74°C (dioxane).FT-IR (ATR, cm^{-1}): 3390 and 3295 (NH_2), 1725 (C=O, ester), 1635 (C=C / C=N), 1525 (NO_2 asym), 1345 (NO_2 sym), 1260 (C–O), 1160, 1105, 1030, 820. ^{1}H NMR (400 MHz, DMSO-d_6): δ 8.22 (d, J = 8.0 Hz, 1H, Ar-H), 8.07 (d, J = 2.0 Hz, 1H, Ar-H), 7.88 (dd, J = 8.2, 2.0 Hz, 1H, Ar-H), 7.62 (d, J = 8.0 Hz, 1H, Ar-H), 7.35 (d, J = 8.0 Hz, 1H, Ar-H), 6.95 (br s, 2H, NH_2), 5.45 (s, 1H, CH), 4.25 (q, J = 7.2 Hz, 2H, OCH_2), 1.30 (t, J = 7.0 Hz, 3H, CH_3).^{13}C NMR (100 MHz, DMSO-d_6): δ 167.0 (C=O, ester), 158.8, 154.3, 149.3, 144.2, 136.6, 130.3, 124.9, 118.5, 111.5, 62.2 (OCH_2), 40.0 (CH2), 14.7 (CH_3). EI-MS (70 eV) m/z (%): 330 $[M+1]^+$, 329 $[M]^+$, 301, 283, 255, 209, 181, 153, 129, 91, 55. Molecular formula: $C_{16}H_{15}N_3O_5$.

synthesis of (11) 2-mercapto-6-(5-nitrobenzofuran-2-yl)nicotinonitrile
The obtained solid was collected and purified by recrystallization from ethanol, yielding brown crystals (68% yield). M.p. 232–34°C (dioxane).FT-IR (ATR, cm^{-1}): 3200 (N–H), 3060 (Ar C–H), 2220 (C≡N), 1600 (C=C / C=N), 1520 (NO_2 asym), 1345 (NO_2 sym), 1200 (C=S).^{1}H NMR (400 MHz, DMSO-d_6): δ 12.20 (br s, 1H, NH), 8.42 (d, J = 2.0 Hz, 1H, Ar-H), 8.18 (dd, J = 9.0, 2.0 Hz, 1H, Ar-H), 8.05 (d, J = 8.0 Hz, 1H, Ar-H), 7.87 (d, J = 8.0 Hz, 1H, pyridine-H), 7.65 (d, J = 8.0 Hz, 1H, Ar-H), 7.28 (d, J = 8.0 Hz, 1H, Ar-H).^{13}C NMR (100 MHz, DMSO-d_6): δ 180.6 (C=S), 158.5, 155.0, 151.3, 146.7, 142.0, 137.1, 129.9, 125.3, 118.5, 111.5.EI-MS (70 eV) m/z (%): 298 $[M+1]^+$, 297 $[M]^+$, 266, 238, 177, 149, 77, 51.
Molecular formula: $C_{14}H_7N_3O_3S$.

synthesis of (13)— S-(3-cyano-6-(5-nitrobenzofuran-2-yl)pyridin-2-yl) benzothioate
The obtained solid was collected and purified by recrystallization from ethanol, yielding dark brown crystals (70% yield). M.p. 277–79°C (dioxane).FT-IR (ATR, cm^{-1}): 3060 (Ar C–H), 2220 (C≡N), 1690 (C=O, S-benzoyl), 1600 (C=C / C=N), 1520 (NO_2 asym), 1345 (NO_2 sym).^{1}H NMR (400 MHz, DMSO-d_6): δ 8.55 (d, J = 2.0 Hz, 1H, Ar-H), 8.30 (dd, J = 8.2, 2.0 Hz, 1H, Ar-H), 8.10 (d, J = 8.0 Hz, 1H, Ar-H), 7.95 (d, J = 8.0 Hz, 1H, pyridine-H), 7.75 (m, 2H, Ph-H), 7.60 (m, 3H, Ph-H), 7.45 (d, J = 8.0 Hz, 1H, Ar-H), 7.30 (d, J = 8.0 Hz, 1H, Ar-H).^{13}C NMR (100 MHz, DMSO-d_6): δ 190.6 (C=O, S-benzoy), 158.5, 154.5, 150.5, 146.5, 137.5, 134.5, 132.5, 129.5, 128.5, 124.5, 118.5, 111.5. EI-MS (70 eV) m/z (%): 402 $[M+1]^+$, 401 $[M]^+$, 373, 296, 105 ($PhCO^+$), 77 (Ph^+). Molecular formula: $C_{21}H_{11}N_3O_4S$.

Synthesis of (14)— S-(3-cyano-6-(5-nitrobenzofuran-2-yl)pyridin-2-yl) ethanethioate
The obtained solid was collected and purified by recrystallization from ethanol, yielding dark orange crystals (78% yield). M.p. 282–84°C (dioxane). FT-IR (ATR, cm^{-1}): 3060 (Ar C–H), 2220 (C≡N), 1695 (C=O), 1600 (C=C / C=N), 1520 (NO_2 asym), 1345 (NO_2 sym).^{1}H NMR (400 MHz, DMSO-d_6): δ 8.45 (d, J = 2.0 Hz, 1H, Ar-H), 8.20 (dd, J = 8.2, 2.0 Hz, 1H, Ar-H), 8.00 (d, J = 8.0 Hz, 1H, Ar-H), 7.80 (d, J = 8.0 Hz, 1H, pyridine-H), 7.55 (d, J = 8.0 Hz, 1H, Ar-H), 7.35 (d, J = 8.0 Hz, 1H, Ar-H), 2.55 (s, 3H, $COCH_3$).^{13}C NMR (100 MHz, DMSO-d_6): δ 193.6 (C=O), 158.5, 154.5, 150.5, 146.5, 137.5, 129.5, 124.5, 118.5, 111.5, 30.4 ($COCH_3$).EI-MS (70 eV) m/z (%): 340 $[M+1]^+$, 339 $[M]^+$, 297 $[M–COCH_3]^+$, 269, 149, 77, 43 (CH_3CO^+). Formula: $C_{16}H_9N_3O_4S$ (M.W. 339).

Synthesis of (15) — 2-(methylthio)-6-(5-nitrobenzofuran-2-yl)nicotinonitrile
The obtained solid was collected and purified by recrystallization from ethanol, yielding brown crystals (71% yield). M.p. 286–89 C (dioxane). FT-IR (ATR, cm^{-1}): 3060 (Ar C–H), 2220 (C≡N), 1600 (C=C / C=N), 1520 (NO_2 asym), 1345 (NO_2 sym), 1260 (C–S).^{1}H NMR (400 MHz, DMSO-d_6): δ 8.42 (d, J = 2.0 Hz, 1H, Ar-H), 8.18 (dd, J = 8.2, 2.0 Hz, 1H, Ar-H), 8.04 (d, J = 8.0 Hz, 1H, Ar-H), 7.85 (d, J = 8.0 Hz, 1H, pyridine-H), 7.62 (d, J = 8.0 Hz, 1H, Ar-H), 7.40 (d, J = 8.0 Hz, 1H, Ar-H), 2.60 (s, 3H, SCH_3).^{13}C NMR (100 MHz, DMSO-d_6): δ 158.5 (C–S / C=N), 155.0, 151.3, 146.7, 142.0, 137.1, 129.9, 125.3, 118.5, 111.5,

Received: 25-05-2026 - **Accepted:** 22-07-2026 - **Published:** 30-07-2026

Attahadi Medical Journal
2026;3(3):358-370
https://doi.org/10.69667/amj.26314

14.7 (SCH_3). EI-MS (70 eV) m/z (%): 313 $[M+2]^+$, 312 $[M+1]^+$, 311 $[M]^+$, 296 $[M–CH_3]^+$, 264, 149, 77, 51. Molecular formula: $C_{15}H_9N_3O_3S$ (M.W. 311).

Molecular Docking Results and Discussion

Validation of the Molecular Docking Protocol

Redocking of the co-crystallized ligand AQ4 into the EGFR binding site successfully reproduced the experimentally determined ligand orientation. Among the generated conformations, pose 3 was selected and exhibited a predicted binding affinity of −7.679 kcal/mol. The heavy-atom RMSD between the selected redocked conformation and the crystallographic AQ4 pose was 1.262 Å. The close positional correspondence of the principal scaffold and peripheral substituents indicates that the selected docking parameters were capable of recovering the experimentally observed binding mode. Because no manual fitting was performed before RMSD determination, the observed agreement originated directly from the docking calculation. On this basis, the docking protocol was considered sufficiently reliable for the subsequent evaluation of compounds 10 and 11 (Figure 3).

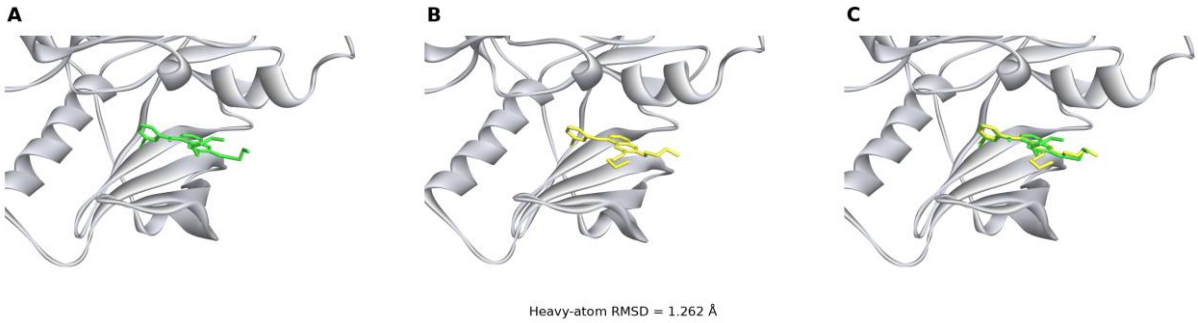

Figure 3. Validation of the molecular docking protocol by redocking the co-crystallized ligand AQ4 into the EGFR tyrosine kinase binding site (PDB ID: 1M17). (A) Experimentally determined crystallographic conformation of AQ4, (B) selected redocked conformation corresponding to pose 3, and (C) superimposition of the crystallographic and redocked AQ4 conformations. The selected redocked pose exhibited a predicted binding affinity of −7.679 kcal/mol and a heavy-atom RMSD of 1.262 Å.

Binding Modes of AQ4 and the Synthesised Compounds

The crystallographic AQ4 ligand occupied the ATP-binding region of the EGFR kinase domain and established a combination of polar, hydrophobic, and π-mediated contacts with the surrounding residues. This experimentally determined binding mode was used as the structural reference for interpreting the predicted orientations of compounds 10 and 11.

Compound 10 was successfully accommodated within the validated AQ4-binding pocket. The selected conformation corresponded to pose 1 and exhibited a predicted binding affinity of −8.305 kcal/mol, representing the most favorable Vina score among the three investigated ligands. Its predicted orientation occupied the same general binding-site volume as AQ4 while adopting a distinct arrangement of peripheral substituents and non-covalent contacts. Compound 11 also occupied the validated EGFR binding region. The selected conformation corresponded to pose 3 and exhibited a predicted binding affinity of −7.876 kcal/mol. Its aromatic and heterocyclic regions showed substantial spatial overlap with the central binding region occupied by AQ4, whereas the terminal substituents adopted a distinct orientation within the cavity. The three-dimensional binding modes of AQ4, compound 10, and compound 11 are comparatively presented in Figure 4. The detailed two-dimensional interaction profiles are shown in (Figure 5).

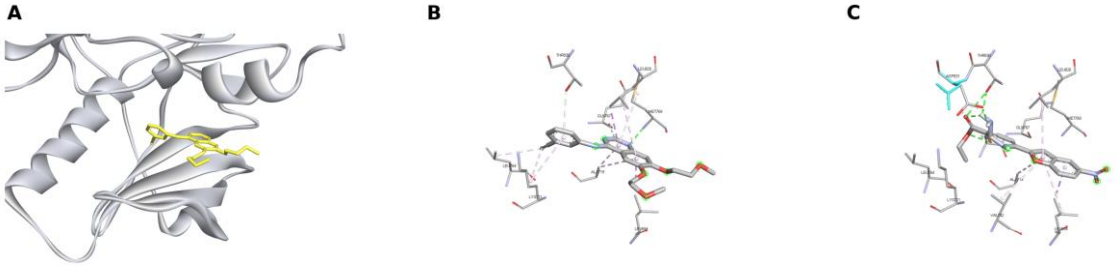

Figure 4. Three-dimensional binding modes of (A) crystallographic AQ4, (B) compound 10, and (C) compound 11 within the EGFR tyrosine kinase binding pocket. The panels illustrate the relative accommodation of the ligands inside the validated binding region. Green dashed lines indicate predicted hydrogen-bonding interactions where displayed.

Received: 25-05-2026 - **Accepted**: 22-07-2026 - **Published**: 30-07-2026

Attahadi Medical Journal
2026;3(3):358-370
https://doi.org/10.69667/amj.26314

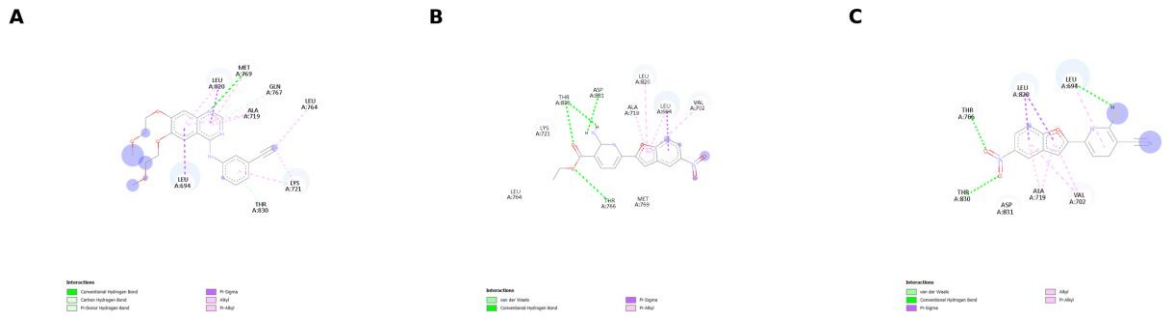

Figure 5. Two-dimensional protein–ligand interaction diagrams of (A) crystallographic AQ4, (B) compound 10, and (C) compound 11 within the EGFR binding pocket. The diagrams illustrate the principal conventional hydrogen bonds, van der Waals contacts, alkyl interactions, and π-mediated contacts identified using BIOVIA Discovery Studio Visualizer version 25.1.0.24284. Interaction colors correspond to the default software legend shown in each panel.

Comparative Docking Analysis

The predicted binding affinities were −7.679, −8.305, and −7.876 kcal/mol for redocked AQ4, compound 10, and compound 11, respectively. Compound 10 produced the most negative docking score, followed by compound 11 and AQ4. The comparative overlay demonstrated that both synthesized compounds occupied the AQ4-defined EGFR binding cavity and retained substantial overlap with the central ligand-binding region (Figure 6).

The difference in docking scores should be interpreted cautiously. A more negative Vina score indicates a more favorable predicted fit within the applied scoring model but does not independently demonstrate stronger biochemical inhibition or experimentally measured binding affinity. Accordingly, these docking results should be considered together with the corresponding biological activity data.

Table 5. Predicted docking results for AQ4 and compounds 10 and 11.

Ligand	Selected pose	Predicted binding affinity (kcal/mol)	Interpretive role
AQ4, redocked	3	−7.679	Validation reference
Compound 10	1	−8.305	Most favorable predicted score
Compound 11	3	−7.876	Favorable predicted score

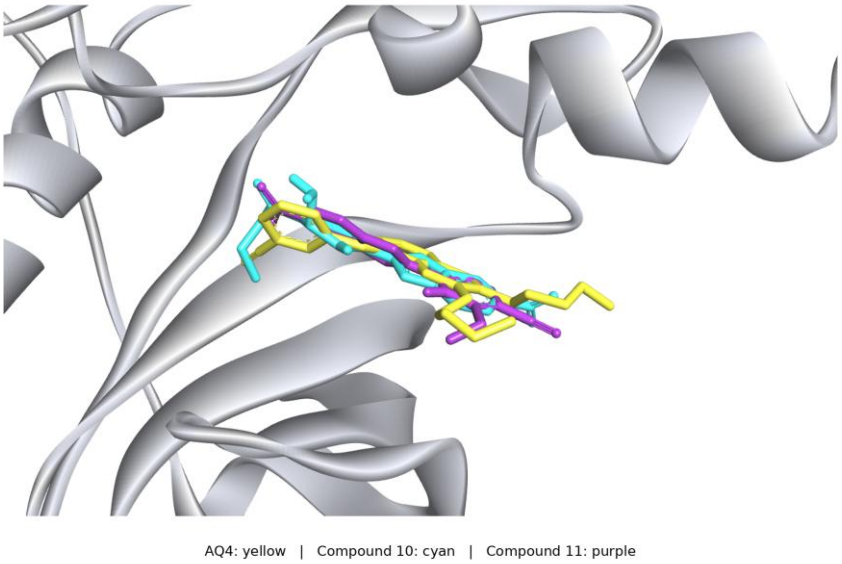

Figure 6. Comparative overlay of crystallographic AQ4 (yellow), compound 10 (cyan), and compound 11 (purple) within the EGFR tyrosine kinase binding cavity. The superimposed conformations illustrate the relative spatial occupation and orientation of the ligands using their original crystallographic or docking-derived coordinates. No independent manual fitting or alignment of the individual ligands was performed.

Docking study summary

Collectively, the validated docking protocol reproduced the crystallographic AQ4 binding mode with a heavy-atom RMSD of 1.262 Å. Both synthesized compounds were accommodated within the AQ4-defined EGFR binding pocket and exhibited

Received: 25-05-2026 - **Accepted**: 22-07-2026 - **Published**: 30-07-2026

predicted binding affinities more negative than that of the selected redocked AQ4 pose. Compound 10 displayed the most favorable predicted docking score of −8.305 kcal/mol, followed by compound 11 at −7.876 kcal/mol and AQ4 at −7.679 kcal/mol. These computational findings provide a structural basis for further interpretation of the biological results; however, docking-derived scores and interactions remain predictive and should not be regarded as direct experimental evidence of EGFR inhibition.

Conclusion

A single 5-nitrobenzofuran-derived enaminone was used as an efficient building block for the synthesis of a diverse set of nitrogen heterocycles. Condensation of the enaminone 3 with 1,3-dicarbonyl reagents and active-methylene nitriles, in the presence of ammonium acetate, gave the substituted pyridines 5–7, the 2-aminonicotinonitrile 9, the dihydropyridine carboxylate 10 and the 2-thioxopyridine-3-carbonitrile 11. The thione/thiol 11then served as a platform for S-functionalisation, providing the benzothioate 13, the ethanethioate 14 and the methylthioether 15. The assigned structures were supported by FT-IR, ^{1}H NMR, ^{13}C NMR and EI-MS data. In the preliminary disc-diffusion screen, compounds 10 and 11 gave the largest inhibition zones among the tested derivatives, especially against the Gram-positive strains. The route therefore offers a practical entry to benzofuran–pyridine hybrids, but MIC/MBC, cytotoxicity and expanded microbiological testing are needed before the compounds can be advanced as antibacterial leads.

The molecular docking study indicated that compounds 10 and 11 can be accommodated within the AQ4-defined binding pocket of EGFR. Successful reproduction of the crystallographic AQ4 orientation supported the reliability of the employed docking protocol. Compound 10 showed the most favorable predicted docking score, while both synthesized compounds maintained plausible binding orientations within the validated active site. These findings support further structure–activity relationship optimization and experimental evaluation of the investigated scaffold against EGFR.

References

1. Stojanović M, Bugarski S, Baranac-Stojanović M. Synthesis of 2,3-dihydro-4-pyridones and 4-pyridones by the cyclization reaction of ester-tethered enaminones. *J Org Chem*. 2020;85(21):13495-13507. doi:10.1021/acs.joc.0c01537
2. Chen XY, Zhang X, Wan JP. Recent advances in transition metal-free annulation toward heterocycle diversity based on the C–N bond cleavage of enaminone platform. *Org Biomol Chem*. 2022;20(12):2356-2369. doi:10.1039/d2ob00126h
3. Zhao P, Wu X, Zhou Y, Geng X, Wang C, Wu YD, Wu AX. Direct synthesis of 2,3-diaroyl quinolines and pyridazino[4,5-b]quinolines via an I_2-promoted one-pot multicomponent reaction. *Org Lett*. 2019;21(8):2708-2711. doi:10.1021/acs.orglett.9b00685
4. El-Khouly OA, Henen MA, El-Sayed MA, Shabaan MI, El-Messery SM. Synthesis, anticancer and antimicrobial evaluation of new benzofuran based derivatives: PI3K inhibition, quorum sensing and molecular modeling study. *Bioorg Med Chem*. 2021;31:115976. doi:10.1016/j.bmc.2020.115976
5. Riyahi Z, Asadi P, Hassanzadeh F, Khodamoradi E, Gonzalez A, Karimi Abdolmaleki M. Synthesis of novel conjugated benzofuran-triazine derivatives: antimicrobial and in-silico molecular docking studies. *Heliyon*. 2023;9(8):e18759. doi:10.1016/j.heliyon.2023.e18759
6. Li J, Liu Q, Li S, Zeng L, Yao J, Li H, Shen Z, Lu F, Wu Z, Song B, Song R. Design, synthesis, antibacterial activity, and mechanisms of novel benzofuran derivatives containing disulfide moieties. *J Agric Food Chem*. 2024;72(18):10195-10205. doi:10.1021/acs.jafc.3c08392
7. Napiórkowska M, Kumaravel P, Amboo Mahentheran M, Kiernozek-Kalińska E, Grosicka-Maciąg E. New derivatives of 1-(3-methyl-1-benzofuran-2-yl)ethan-1-one: synthesis and preliminary studies of biological activity. *Int J Mol Sci*. 2024;25(4):1999. doi:10.3390/ijms25041999
8. Wu H, Zhao H, Lu T, Xie B, Niu C, Aisa HA. Synthesis and activity of aurone and indanone derivatives. *Med Chem*. 2023;19(7):686-703. doi:10.2174/1573406419666230203105246
9. Kassab RM, Zaki ME, Abo Dena AS, Al-Hussain SA, Abdel-Aziz MM, Muhammad ZA. Novel set of highly substituted bis-pyridines: synthesis, molecular docking and drug-resistant antibacterial profile. *Future Med Chem*. 2022;14(24):1881-1897. doi:10.4155/fmc-2022-0196
10. Rizwan M, Noreen S, Asim S, Liaqat Z, Ibrahim H, Talib R. A comprehensive review on synthesis and antimicrobial evaluation of substituted-arylideneamino-5-(5-chlorobenzofuran-2-yl)-1,2,4-triazole-3-thiol derivatives/Schiff bases. *J Fluoresc*. 2024;35:3733-3761. doi:10.1007/s10895-024-03817-3
11. AlDifar H, Baaiu B, Elabbar F. Targeted cytotoxicity and docking studies of novel benzenesulfonamide derivatives against human cancer cell lines. *AlQalam J Med Appl Sci*. 2026:1184-1202. doi:10.54361/ajmas.269509
12. Stamos J, Sliwkowski MX, Eigenbrot C. Structure of the epidermal growth factor receptor kinase domain alone and in complex with a 4-anilinoquinazoline inhibitor. *J Biol Chem*. 2002;277(48):46265-46272. doi:10.1074/jbc.M207135200
13. Trott O, Olson AJ. AutoDock Vina: improving the speed and accuracy of docking with a new scoring function, efficient optimization, and multithreading. *J Comput Chem*. 2010;31(2):455-461. doi:10.1002/jcc.21334
14. Eberhardt J, Santos-Martins D, Tillack AF, Forli S. AutoDock Vina 1.2.0: new docking methods, expanded force field, and Python bindings. *J Chem Inf Model*. 2021;61(8):3891-3898. doi:10.1021/acs.jcim.1c00203
15. Morris GM, Huey R, Lindstrom W, Sanner MF, Belew RK, Goodsell DS, Olson AJ. AutoDock4 and AutoDockTools4: automated docking with selective receptor flexibility. *J Comput Chem*. 2009;30(16):2785-2791. doi:10.1002/jcc.21256
16. Dassault Systèmes BIOVIA. *Discovery Studio Visualizer*. Version 25.1.0.24284. San Diego (CA): Dassault Systèmes; 2024.

***Received**: 25-05-2026 - **Accepted**: 22-07-2026 - **Published**: 30-07-2026*